Title:

Coarse-grained meandering distributive fluvial system of the basal Cedar Mountain Formation, USA

Running Title:

DFS of the basal Cedar Mountain Formation

Phillips, Stephen P.[1]; Howell, John A.[2]; Hartley, Adrian J.[2]; Chmielewska, Magda[2]

[1]Department of Geological Sciences, S-389 Eyring Science Center, Brigham Young University, Provo, UT 84602, USA

[2]Department of Geology and Petroleum Geology, Meston Building, University of Aberdeen, AB24 3UE, United Kingdom

the.geologist@outlook.com

john.howell@abdn.ac.uk

a.hartley@abdn.ac.uk

magda.chmielewska@abdn.ac.uk

Keywords: facies analysis, architectural analysis, foreland basin, fluvial planform, distributive fluvial system

ABSTRACT

The analysis of downstream changes in ancient fluvial systems can better inform depositional models for foreland-basin systems. Herein we analyze the basal deposits of the Early Cretaceous Cedar Mountain Formation of Utah to better understand the variety of fluvial deposits present and to develop a depositional model for the Sevier foreland basin. We also evaluate the long-held interpretation of a braided origin for these deposits and document numerous examples of point-bar deposition in highly sinuous meandering rivers by analysis of large (20 to 60 km^2) plan-view exposures. These plan-view exposures allow comparisons between planform and cross-sectional geometries.

The study utilizes outcrop data, virtual outcrop models, and satellite imagery to develop a facies model and analyze the architecture of channel bodies in the Buckhorn Conglomerate and Poison Strip Sandstone of the Cedar Mountain Formation. We document downstream (west to east) decreases in lateral channel migration, sinuosity, channel amalgamation, grain size, and percent of fluvial channel facies (conglomerate and sandstone). Fluvial channel deposits occur arranged into larger stratal bodies: multistory-multilateral channel bodies that are dominantly composed of clast-supported conglomerate in the west to a mix of multistory, multilateral and isolated channel bodies composed of matrix-supported conglomerate in the east. The median width of highly sinuous point bars is similar across the field area (344 m to 477 m), but the inclusion of narrower (median = 174 m), low-sinuosity bar elements in the east indicates an overall reduction in lateral channel migration and sinuosity downstream. Net-to-gross values range from 100% in much of the western outcrops to as low as 38% in the east. Paleocurrent analysis reveals a transverse (west to east) paleoflow for the study interval that merges with axial (south-north) paleoflow near the Utah-Colorado state line. We estimate 10^4 m^3/s-scale discharge and 10^6 kilometer-scale drainage area for axial rivers based on paleohydraulic analysis which represents a significant part of the Early Cretaceous continental-scale drainage.

The observed downstream trends in lateral channel migration, sinuosity, channel amalgamation, grain size, and net-to-gross for the basal Cedar Mountain Formation are consistent with expected trends for sinuous single-thread distributive fluvial systems and are similar to observed trends in the Jurassic Morrison Formation. Medial (Buckhorn Conglomerate) to distal (Poison Strip Sandstone) zones are preserved and span the forebulge to backbulge depozones of a foreland-basin system. Postulated deposits of the proximal distributive fluvial system have been removed during erosion of the foredeep depozone. The easternmost Poison Strip Sandstone and coeval Burro Canyon Formation represent deposits of an axial system at which western-sourced distributive fluvial systems end. Distributive fluvial systems dominate modern foreland basins, and this study suggests that they may constitute a significant proportion of ancient successions.

INTRODUCTION

Fluvial planform has a controlling influence over the geometry of preserved channel body elements in the sedimentary record (e.g., Miall, 2010). A proper understanding of the relationship between planform geometry and cross-sectional geometry of fluvial deposits is essential in the reconstruction of ancient fluvial systems (e.g., Ielpi and Ghinassi, 2014; Hartley et al., 2015; Bhattacharya et al., 2015; Owen et al, 2015) and aids in the estimation of variables such as discharge, drainage area, and slope (e.g., Bridge and Mackey, 1993; Bhattacharya and MacEachern, 2009; Bhattacharya et al., 2016). Despite misconceptions in the past (e.g., Miall, 1977; Allen, 1983; Cant, 1982; Miall, 2010), it is now clearly understood that coarse-grained to pebbly channel fills are in no way restricted to braided fluvial systems (e.g., Clayton and Pitlick, 2007; Métivier and Barrier, 2012; Braudrick, 2013). Interpretations regarding discharge, slope, sediment supply, paleogeographic location, depositional and tectonic modelling, etc. are then based on this assumption, making accurate interpretations of planform essential (e.g., Bridge and Mackey, 1993; Blum et al., 2013; Ielpi and Ghinassi, 2014; Hartley et al., 2015; Bhattacharya et al., 2015). Additionally, an accurate description of the geometry of preserved elements aids in predictions of reservoir geometry, leading to efficient recovery of subsurface resources such as oil and natural gas.

The aim of this study is to evaluate the relationship between planform exposure and cross-sectional outcrop in a system that has been historically identified as a braided fluvial system. Our objectives are to determine the dominant fluvial planform for the system by analyzing channel body elements in plan view and cross-sectional view, estimate palaeohydraulics, and build a depositional model for coarse-grained alluvium from the Early Cretaceous of Utah. The succession has been widely interpreted as the deposits of an amalgamated braided fluvial system (e.g., Young, 1973; Yingling, 1987; Heller and Paola, 1989; Currie, 1997; Ayers, 2004; Stikes, 2007). We assess the assumption that braided rivers dominated during the deposition of the lower Cedar Mountain Formation through analysis of outcrops, satellite imagery, virtual outcrop models, and paleocurrent data. Exceptional plan-view exposures that cover large areas (20 to 60 km^2) allow identification of planform geometries, and virtual outcrop models allow reconstruction of architecture in two and three dimensions. We also challenge the validity of planform interpretations derived solely from vertical outcrop exposure (e.g., Ethridge, 2011; Ghinassi et al., 2013; Ghinassi et al., 2014; Ielpi and Ghinassi, 2014; Ghinassi and Ielpi, 2015; Hartley et al., 2015; Swan et al., 2018). High-quality plan-view outcrops facilitate the interpretation of fluvial planform (Ielpi and Ghinassi, 2014; Ghinassi and Ielpi, 2015; Hartley et al., 2015; Swan et al., 2018).

Distributive fluvial systems (DFSs) are purported to dominate modern and ancient basins, including foreland-basin systems (e.g., Hartley et al., 2010; Weissmann et al., 2010; Davidson et al., 2013; Rittersbacher et al., 2014; Owen et al., 2015; Primm et al., 2018; Owen et al., 2019). We compare degree of channel amalgamation, changes in sinuosity, and variation in paleocurrents of modern sinuous single-thread DFSs (Davidson et al., 2013) with the basal Cedar Mountain Formation to test the hypothesis that the basal Cedar Mountain Formation represents a DFS.

GEOLOGICAL SETTING

Study Area

The study area in east-central Utah (Fig. 1) has a nearly continuous vertical outcrop of the basal Cedar Mountain Formation extending hundreds of kilometers, as well as extensive plan-view exposures on the flanks of the San Rafael Swell (Fig. 1: GR, GRCR, SWGR, SEGR).

Lithostratigraphy

The basal member of the Cedar Mountain Formation on the western flank of the San Rafael Swell is the Buckhorn Conglomerate (Stokes, 1944; Kirkland et al., 2016)(Fig. 2). East of the San Rafael Swell, however, basal Cedar Mountain Formation deposits are the lowermost Yellow Cat Member and the overlying Poison Strip Sandstone (Kirkland et al., 1997; Kirkland et al., 2016)(Fig. 2). The time-equivalent Cedar Mountain and Burro Canyon formations are arbitrarily separated by the Colorado River (Stokes, 1952)(Fig. 1). Basal Cedar Mountain Formation deposits unconformably overlie the Jurassic Brushy Basin Member of the Morrison Formation and are overlain everywhere by the Aptian to Albian Ruby Ranch Member of the Cedar Mountain Formation (Fig. 2). The Cedar Mountain Formation has been the focus of considerable paleontological research (see Kirkland et al, 2016).

The Buckhorn Conglomerate has been interpreted as filling paleovalleys incised into the underlying Morrison Formation (Currie, 1997, 1998). This conclusion was primarily based on stratigraphic relationships and isopach mapping of Buckhorn Conglomerate deposits on the northern side of the Uinta Basin (Currie, 1997, 1998). However, significant differences exist between the Buckhorn Conglomerate deposits of the northern Uinta Basin and the deposits of the northern San Rafael Swell near the type section, a separation of 170 km (Fig. 1). Assuming continuity between the western and eastern flanks of the San Rafael Swell, the Buckhorn Conglomerate has a much larger lateral extent, covering over 2,000 km^2 in the north part of the San Rafael Swell alone, and the mapped paleovalley in the northern Uinta Basin is approximately 30 km wide (Currie, 1997, 1998). However, lateral pinch-out of paleovalley deposits against paleovalley walls has yet to be demonstrated in the San Rafael Swell, and deposits of the Swell cannot be positively correlated with those of the northern Uinta Basin.

The age of the basal Cedar Mountain Formation is poorly constrained. Detrital-zircon ages for the Poison Strip Sandstone indicate that it is no older than 124 to 130 Ma (Mori, 2009), and a U/Pb age from a carbonate at the very top of the underlying Yellow Cat Member provides a lower bound at 119.4 +/- 2.6 Ma (Ludvigson et al., 2010)(Fig. 2). No ages exist for the Buckhorn Conglomerate, but it is thought to be at least partially time-equivalent to the Poison Strip Sandstone based on stratigraphic relationships (Kirkland and Madsen, 2007).

Tectonic Models

The upper Cedar Mountain Formation (Ruby Ranch and Mussentuchit members) was deposited in a developing foreland basin system east of the Sevier fold and thrust belt (Armstrong, 1968; Lawton et al., 1997; Currie, 1997). These deposits thicken into the foredeep depozone (≈ 1100 m, westward) and thin over the forebulge depozone (≈ 50 m, eastward; DeCelles and Giles, 1996; DeCelles and Currie, 1996; Currie, 1997)(Fig. 3). They have been interpreted as floodplain and tributary fluvial channel successions deposited as part of an aggradational, low-to-moderate-sinuosity system (Currie, 1997, 1998) or as a progradational sinuous single-thread DFS (Holmes, 2017; Cardenas et al., 2020; Phillips et al., 2021).

The lower Cedar Mountain Formation is composed of the Buckhorn Conglomerate, the Poison Strip Sandstone, and the Yellow Cat Member. There is an increase in sediment thickness away from the mountain belt, eastward into a postulated backbulge depozone (500% increase; Royse, 1993; DeCelles and Giles, 1996; DeCelles and Currie, 1996; Currie, 1997; Currie, 2002; DeCelles, 2004; Hunt et al., 2011)(Fig. 3). An alternative thermal-uplift mechanism, based on outcrop observations and flexural modelling, has also been proposed (Heller and Paola, 1989; Heller et al., 2003). Additionally, the Yellow Cat Member is interpreted to have been deposited very slowly and contains significant hiatuses (Joeckel et al., 2017; Joeckel et al., 2019). These characteristics are attributed to the interaction of the fluvial systems with localized salt tectonics in the Paradox Basin (Kirkland, 2017; Joeckel et al., 2017). For this reason, it was not included in this study.

METHODS

To characterize the variety and architecture of fluvial deposits of the basal Cedar Mountain Formation, field data were collected at locations spanning the northern part of the San Rafael Swell and the southern Uinta Basin (Fig. 1). Data collected includes photographs (all locations), measured sections (nine locations), nine virtual outcrops (Buckley et al., 2008), and paleocurrent measurements (eight locations, 1,474 measurements). Paleocurrent measurements were evaluated using rose diagrams created with Stereonet 10 (Allmendinger, 2020). Virtual outcrops were generated using photogrammetry on c. 12,000 images collected using a Phantom 4 Pro UAV and were interpreted in LIME (Buckley et al., 2019) to map the vertical and lateral organization of architectural elements. Virtual outcrops were also used to measure channel-body width and thickness (n = 60) as well as channel-belt width and thickness (n = 10).

Plan-view outcrops of the basal Cedar Mountain Formation deposits are present over the entire field area, but exceptional examples exist for the Buckhorn Conglomerate on the west flank of the San Rafael Swell near its type section at Cedar Mountain and on the east flank of the San Rafael Swell along the Green River Cutoff Road (CM and GRCR, Fig. 1). Similarly, the Poison Strip Sandstone is exceptionally well exposed in plan view within 20 km of the city of Green River, Utah (SWGR and SEGR, Fig. 1). Plan-view exposure allows the measurement of width (n = 56) and length (n = 36) of bar elements as well as the radius of curvature (n = 40). Paleocurrent measurements taken in the field verify interpretations of accretion directions made via satellite imagery.

FACIES ANALYSIS

Several workers have provided facies analyses for the Buckhorn Conglomerate (Conley, 1986; Roca, 2003; Ayers, 2004; Roca and Nadon, 2007). In addition, Stikes (2007) produced a detailed facies and architectural analysis of the Poison Strip Sandstone in the outcrop belt north of Moab, Utah. These facies schemes were developed for local areas in our larger study area. The facies scheme introduced here is similar to that developed in Stikes (2007), and it applies across the study area. Eleven facies are identified (Fig. 4) and grouped into two broad facies associations; FA1 – floodplain and FA2 – fluvial channel (Tables 1 and 2).

FA1 – Floodplain

Description.--- Deposits of FA1 are primarily variegated, and typically mottled mudstone with lesser amounts of nodular and bedded carbonate and thin sandstone beds (Fig. 4A, B). Bedded carbonate and nodular carbonate horizons are laterally continuous and are often present below the scoured basal surface of FA2 (Fig. 4B). Nodules are typically grouped in crudely vertical columns (Fig. 4B). Sandstone beds are cross-stratified, but it can often be difficult to discern sedimentary structures. They are commonly covered by mudstone and are best exposed below cliffs of FA2 (Fig. 4A). They can be laterally continuous for more than a kilometer and can merge laterally with deposits of FA2.

Interpretation.--- These deposits are interpreted as overbank fines, palustrine and lacustrine carbonate, calcic paleosols, and crevasse splays, all deposits common to floodplain environments (Kirkland et al., 1997; Kirkland et al., 2016). The presence of calcic horizons may suggest an arid to semiarid environment (Kirkland et al., 1997; Montgomery et al., 2013; Kirkland et al., 2016).

FA2 – Fluvial Channels

Description.--- FA2 is dominantly composed of poorly sorted extrabasinal (Hunt et al., 2011) granule to cobble conglomerate and pebbly sandstone (Figs. 4C-F, 5). Conglomerate and sandstone are commonly interbedded. Grain size decreases and the relative amount of sand increases eastward across the study area. Trough cross-stratification is the dominant type of bedding at all locations, and it is common in both conglomerate and sandstone beds (Figs. 4C-F, 5). The upper parts of the Poison Strip Sandstone are in some places composed of ripple cross-stratified and planar-laminated sandstone (Fig. 4G). Horizontal and sinuous tubular burrows are present as well as root traces that extend downward from the upper surfaces of the uppermost beds (Fig. 4H). Nodules of authigenic calcium carbonate are common just above basal scoured surfaces, and these nodules are similar in appearance to underlying nodules found in FA1 (Fig. 4I). FA2 commonly overlies beds of this same nodular carbonate (Fig. 4B). Master bedding surfaces dip at an angle that is perpendicular to the direction of paleoflow structures recorded from cross-bedding, ripples, and primary current lineation. Plan-view exposures highlight this and indicate that master bedding surfaces are arcuate, typically forming major arcs (Fig. 6). Master bedding surfaces extend from the upper surfaces to the basal surfaces of individual sand or conglomerate bodies. These deposits have an overall lensoidal geometry and always overlie scoured surfaces.

Interpretation.--- We interpret these deposits to be the product of migrating fluvial channels with point bars as the dominant barform (e.g., Clayton and Pitlick, 2007; Miall, 2010; Ielpi and Ghinassi, 2014; Fig. 6). Dipping master bedding surfaces are interpreted as lateral-accretion surfaces. Paleocurrents oriented roughly parallel to the trend of accretion surfaces are indicative of lateral accretion and are consistent with the interpretation of a point-bar deposit (Fig. 6). Paleocurrents from the basal Cedar Mountain Formation indicate a flow direction toward the east-northeast suggesting a source area to the west and southwest consistent with previous studies (Craig, 1981; Currie, 2002; Dickinson and Gehrels, 2008; Hunt et al., 2011)(Fig. 1). The commonness of cobbles is compatible with high flow velocities in the western part of the study area. The decrease in grain size and increase in the amount of sand eastward indicates that the coarsest fraction was deposited closer to the source area. Burrows and rooting, preferentially located on ripple or trough cross-stratified bar tops, indicate colonization of the bar by plants and animals as migration of the channel continued (e.g., Cant, 1982; Bridge, 2006; Miall, 2010). Carbonate nodules in basal lags are likely derived from underlying soils or palustrine carbonates (Ludvigson et al., 2010, 2015; Kirkland et al., 2016; Joeckel et al., 2017, 2019).

ARCHITECTURAL ANALYSIS

Channel bodies are commonly arranged in multistory, multilateral, or combined multistory-multilateral architectures (Figs. 5, 7). Multistory bodies are typically two or three stories in height and we observed a maximum of seven stories. Lateral extent of multilateral bodies ranges from 180 m to at least 15 km wide, and they are not always multistory. Lateral extent of amalgamated bodies commonly exceeds the width of virtual outcrop (> 2.5 km). In these situations, maximum width (15 km) is estimated from satellite imagery. Multistory bodies are bounded above and below by FA1 deposits of the Ruby Ranch and Yellow Cat members, respectively. FA1 deposits are also found in the Poison Strip Sandstone and Buckhorn Conglomerate with net-to-gross values ranging from 38% to 100%. Isolated channel bodies, which are less common than multistory or multilateral deposits, are completely encased in FA1 deposits. Moreover, isolated channel bodies are not found in the Buckhorn Conglomerate (Fig. 7).

Two examples of multistory architecture are presented in Figures 8 and 9 with three-dimensional exposure (both cliff-face and plan-view). Two stacked point-bar elements are present at Utahraptor Ridge (URR, Fig. 1) with paleoflow parallel (length) and paleoflow transverse (width) exposures (Fig. 7D) showing the accretion surfaces of each point-bar element (Fig. 8). Length-view exposures of story 2 have flat to concave downward accretion surfaces that delineate the upstream and central parts of the point-bar element (e.g., Ghinassi and Ielpi, 2015)(Fig. 8D). Width- and plan-view exposures of story 2 reveal the expansion of a point bar (Fig. 8B, F, G). At Green River Airport (GRA, Fig. 1), plan-view exposure extends to the cliff edge and illustrates the expansion of a point bar (story 2, Fig. 9) within a multistory-multilateral deposit. Additionally, isolated channel bodies are present at this location below the multistory-multilateral deposits (Fig. 9A, B). A 170 m part of a 2.7 km-wide single-story, multilateral deposit from the Buckhorn Conglomerate is shown in Figure 10. Accretion surfaces indicate north-northeast expansion of a point bar with paleocurrent measurements oriented east-southeast (perpendicular) to accretion surfaces (Fig. 10C).

DIMENSIONAL DATA

Dimensional data were collected via two methods; satellite imagery and virtual outcrop models. Satellite data provide information about fluvial planform and makes measurements of bar length, width, and radius of curvature possible. Measurements of thickness and apparent width of bars and channel belts were made using virtual outcrop models.

Satellite Data – Fluvial Planform

Large (20 to 60 km^2) plan-view exposures of both members facilitate the identification of fluvial planforms (Fig. 6). Large point-bar elements (as much as 740 m in width) with a median radius of curvature of 222 m (n = 20) are the dominant barform in the Buckhorn Conglomerate of the San Rafael Swell (Table 3; Figs. 6, 7). Two fundamental planforms are represented in the Poison Strip Sandstone east of the San Rafael Swell; (1) large point-bar elements (as much as 1000 m in width) with a median radius of curvature of 284 m (n = 18; Table 3; Figs. 6, 8, 9) and (2) laterally accreting bars with accretion surfaces that form a minor arc. For the latter case, low-sinuosity channel belts are inferred from a reduction in width (median of 174 m; n = 14) and the absence of a major arc in planform. Dimensions of preserved point-bar elements are similar between members (Table 3). A qualitative trend was taken for each channel belt as a substitute for paleocurrent data by drawing a straight line along the length of the bar or channel belt and taking an azimuth measurement. Trend measurements agree with actual paleocurrent measurements and indicate an eastward directed paleoflow for the Buckhorn Conglomerate and a northeastern paleoflow for the Poison Strip Sandstone (Fig. 1).

Virtual Outcrop Data

Width and thickness values obtained for channel bodies in the virtual outcrop models indicate that the channel bodies are similar in size between members (Table 4). The median width for the Buckhorn Conglomerate is 204 m, and for the Poison Strip Sandstone the median is 228 m. The median thickness for the Buckhorn Conglomerate and Poison Strip Sandstone is 5.7 and 4.0, respectively. Apparent width has been corrected to true width using mean paleocurrent values for three separate areas: (1) Buckhorn Conglomerate of the western San Rafael Swell, (2) Buckhorn Conglomerate of the Eastern San Rafael Swell, and (3) the Poison Strip Sandstone east of the San Rafael Swell. To show the range of possible widths, corrections using paleocurrent values of one standard deviation from the mean are also shown (Fabuel-Perez et al., 2009; Table 3). Two outliers in the Poison Strip Sandstone increase the upper range of thickness values (13.8 m and 18.1 m). The outliers in the Poison Strip Sandstone are important because they represent the deepest channels and provide an estimate of maximum discharge for the whole system.

PALEOHYDRAULICS

On the basis that the fluvial planform for the basal Cedar Mountain Formation was dominantly meandering, paleodischarge can be estimated using the thickness of preserved point-bar elements. Channel-body thickness was measured in virtual outcrop models. The thickest channel body is located at Owl Draw Road (18.1 m; ODR, Fig. 1) and is interpreted to represent a trunk river. Our thickest preserved channel body is, however, a significant outlier relative to the median channel depth, so a median bar thickness (4.7 m) is also reported (Table 5).

To calculate paleodischarge, cross-sectional area and flow velocities must be estimated. Cross-sectional area is first calculated by multiplying the paleochannel depth and width. Bar height is estimated to be 90% of bankfull channel depth (Bridge and Mackey, 1993)(Equation 1). We use this correction in our calculations as well as an adjustment (0.65) for the shape of the channel (Bhattacharya and MacEachern, 2009)(Equation 2). Estimates of channel width were made using empirical relationships reported in Bridge and Mackey (1993)(Table 5). The width of modern channels can vary significantly over short reaches (Phillips et al., 2021). Using several empirical relationships provides a range of estimates that may capture the expected variability in channel width.

Estimates of minimum and maximum flow velocities can be obtained from phase diagrams of Rubin and McCulloch (1980) if flow depth and the dominant bedform is known (Fig. 11A). The thickest channel body is composed of sandstone with dunes as the dominant bedform. The range of possible velocities for the thickest channel is shown in Figure 11A (0.68 to 1.68 m/s). A minimum discharge estimate is calculated by using the minimum estimated flow velocity and the minimum estimate of channel width (Table 5). Similarly, a maximum discharge estimate is calculated with maximum velocity and width (Table 5). We also calculated "average" discharges by using a velocity of 1 m/s and an average of the three width estimates (707 m, max; 75 m, median; Table 5). Discharge is calculated by multiplying cross-sectional area by flow velocity (equation 3).

1. $d_b = h / 0.9$ Bridge and Mackey, 1993
2. $A = d_b * w_c * 0.65$ Bhattacharya and MacEachern, 2009
3. $Q = U*A$

Where d_b is bankfull channel depth, h is preserved bar thickness, w_c is channel width, A is cross-sectional area, U is velocity, and Q is discharge.

A better understanding of paleodrainage can be obtained from known relationships between discharge and drainage area (e.g., Blum et al., 2013; Bhattacharya et al., 2016). Bankfull discharge and drainage area are positively correlated (Matthai, 1990; Mulder and Syvitski, 1995; Davidson and Hartley, 2010; Blum et al., 2013). Similarly, point-bar thickness and drainage area are also positively correlated (Blum et al., 2013). We use the relationship presented by Blum et al. (2013) to estimate drainage area for our "average" discharge for the thickest channel and have shown this in Figure 11B (slightly less than 1 x 10^6 km^2). This estimate of drainage area agrees well with an estimate obtained via the relationship between point-bar thickness and discharge (Fig. 11C). Drainage area for fluvial systems of this time interval (125-113 Ma) has been estimated based on detrital-zircon provenance and indicates continental-scale drainage of greater than 7.5 million km^2 (Blum and Pecha, 2014). This continental-scale drainage area is composed of several constituent drainages that ultimately flowed into the Boreal Sea (Blum and Pecha, 2014). Our drainage-area estimate of approximately 900 thousand km^2 is a significant part (12%) of the overall continental-scale drainage.

DISCUSSION

Variability of Planform in Time and Space

Modern rivers can have highly variable planforms in time and space (Ethridge, 2011). Rivers are known to change planform over short stretches (e.g., Bridge, 2006; Ethridge, 2011). They can also change planform over short periods of time (e.g., Lunt and Bridge, 2004). Additionally, features common in one kind of system are occasionally found in other systems: Point bars in a braided system are a good example of this (e.g., Miall, 1977; Brice, 1982; Ethridge, 2011). The degree of variability apparent in many modern streams is difficult to assess in ancient deposits (Ethridge, 2011). Furthermore, predictions of fluvial planform from two-dimensional outcrop may not be accurate (Hartley et al., 2015). Stikes (2007) observed that vertical and architectural profiles of the Poison Strip Sandstone gave “mixed signals” regarding the type of planforms. Vertical profiles, for example, appeared to indicate a braided system, yet his data were inconclusive. Three-dimensional exposures, such as those we present (Figs. 6, 8-10), permit the most accurate interpretations of planform (e.g., Bhattacharya et al., 2015; Hartley et al., 2015; Swan et al., 2018).

Plan-view images of both the Buckhorn Conglomerate and the Poison Strip Sandstone reveal a dominance of point-bar deposits, and we have not documented any examples of downstream accretion in the parts of outcrop visible in satellite imagery. If these were simply point bars in a braided fluvial system, many examples of downstream accretion, a common component of braided systems, should be present (e.g., Miall, 1977; Allen, 1983; Cant, 1982; Miall, 2010). Therefore, we conclude that the youngest rivers of the basal Cedar Mountain Formation were meandering rivers of varying sinuosity and that planform did not vary significantly across the field area.

Generally, satellite imagery provides only plan-view images of the uppermost story at any given location, but several examples of stacked point bars exist (see Fig. 6 B, E, F, and G). Two of these locations were checked in the field to verify that the bars are indeed stacked rather than being laterally adjacent (Fig. 6 E, G). Additionally, at the Utahraptor Ridge location (URR, Fig. 1) we have analyzed virtual outcrop imagery which provides both bar length and width views of stacked point-bar deposits (Fig. 8). Lateral accretion is indicated by paleocurrent direction perpendicular to dipping accretion surfaces. Point-bar width views show lateral-accretion surfaces that extend from the top of the bar to the base. Length views show broadly concave-down accretion surfaces. No differences in planform were observed between stories. All of these examples indicate that meandering planform persists below the uppermost story, and we conclude that meandering planform was persistent throughout deposition of the lower Cedar Mountain Formation.

Distributive Fluvial Systems

Comparison with Modern Distributive Fluvial Systems.--- Modern foreland basins such as the Himalayan, Andean and Alaskan foreland basins are dominated by DFSs which end at, and are tributary to, axial rivers (e.g., Gupta, 1997; Shukla et al, 2001; Horton and DeCelles, 2001; Hartley et al., 2010; Weissmann et al., 2010). Terminations may be perpendicular or oblique to the axial system (Phillips et al., 2021). Lateral channel migration is predominant in the proximal to medial parts of modern sinuous, single-thread anabranching DFSs (Davidson et al., 2013). Additionally, expansion of meanders leads to levee breaches and associated crevasse-splay deposition (Davidson et al., 2013; Valenza et al., 2020). Distal DFS channels have more limited lateral migration, exhibit lateral displacement by avulsion, contain vertical aggradation, and are encased in significant floodplain deposits (Weissmann et al., 2010; Davidson et al., 2013; Weissmann et al., 2013; Weissmann et al., 2015).

Basal Cedar Mountain Formation deposits share several characteristics with modern single-thread DFSs such as significant lateral channel migration by expansion of point bars (Figs. 6, 8-10) in the more proximal part of the study area (100% high sinuosity) and the presence of significant crevasse-splay deposits (Fig. 7). The presence of narrow channel belts in the Poison Strip Sandstone (44% low sinuosity) indicates a shift to more limited lateral migration in the distal part of the system. Net-to-gross values are 100% over much of the San Rafael Swell and as low as 38% east of the San Rafael Swell, indicating an increase in floodplain deposits eastward. Amalgamation of channel bodies is common throughout the field area, but isolated channels are limited to the Poison Strip Sandstone.

The presence of a dominantly transverse or eastward paleocurrent for the Buckhorn Conglomerate suggests a westward source area whereas the Poison Strip Sandstone has an east to northeast directed paleocurrent (e.g., Craig, 1981; Currie, 1998; Dickinson and Gehrels, 2008; Hunt et al., 2011)(Figs. 1, 12). Published paleocurrent data for the coeval Burro Canyon Formation indicate a northward paleoflow (Craig, 1981; Aubrey, 1992; Dickinson and Gehrels, 2008)(Fig. 12). Provenance studies confirm that sediment in the Buckhorn Conglomerate was sourced from thrust sheets west of the study area (Dickinson and Gehrels, 2008; Lawton et al., 2010; Hunt et al., 2011; Fig. 12). In contrast, a progressive west-to-east increase in Cordilleran arc-derived sediment sourced from the south is preserved in the Poison Strip Sandstone and Burro Canyon Formation (Dickinson and Gehrels, 2008; Lawton et al., 2010; Hunt et al., 2011)(Fig. 12).

A comprehensive dataset of catchment size exists for the 27 major drainages in the modern Himalaya with a median size of 11,688 km^2 (range of 9,526 to 255,929 km^2; Bookhagen and Burbank, 2010). We have estimated drainage area for trunk river deposits in the axial (eastern) part of the study area (slightly less than 1×10^6 km^2; Fig. 11B). These trunk rivers likely represent the combined flow of multiple smaller catchments to the west. Median bar thickness may better characterize western-sourced DFS. Using the median bar thickness of 4.7 m (Table 5), drainage areas for these smaller constituent drainages would be on the order of 10^4 km^2, in line with values obtained from the Himalaya.

Comparison with Ancient Distributive Fluvial Systems.--- DFSs have also been documented in ancient foreland basins (e.g., Owen et al., 2015; Primm et al., 2018; Owen et al., 2019). Owen et al. (2015) quantified downstream trends in the mixed meandering to braided Salt Wash DFS in the Morrison Formation and found that significant variation exists from proximal to distal position on the DFS. Grain size, net-to-gross ratios, degree of amalgamation, belt thickness, and story thickness all decrease downstream (Owen et al., 2015). Other types of DFSs, including sinuous, single-thread ones, may exhibit variation in such trends (Davidson et al., 2013).

In spite of a difference in fluvial planform, deposits of the basal Cedar Mountain Formation compare favorably with those of the Morrison Formation (Owen et al., 2015). Grain-size trends were not quantified in this study, but we can qualitatively report that the ratio of pebbles to sand in channel bodies decreases eastward. The Buckhorn Conglomerate of the San Rafael Swell is dominantly composed of extrabasinal, clast-supported pebble conglomerate. In contrast, the Poison Strip Sandstone is dominantly composed of matrix-supported, pebbly sandstone. Other workers have documented a similar trend of decreasing grain size eastward (Heller and Paola, 1989). As mentioned above, net-to-gross values decrease downstream (100 to 38%) with an accompanying decrease in channel amalgamation as evidenced by the increase in isolated channel bodies. Unlike the fluvial deposits of the Morrison Formation, there is no systematic decrease in story (bar) or channel-belt thickness across the field area. The thickness of the basal Cedar Mountain Formation is relatively consistent across the field area.

We suggest that the deposits of the Buckhorn Conglomerate and Poison Strip Sandstone in our field area are the medial to distal parts of DFSs (Fig. 12) with apices in the thrust belt to the west and southwest. These DFSs merge with an axial system (eastern Poison Strip Sandstone and Burro Canyon Formation) near the Utah-Colorado state line (Fig. 12).

CONCLUSIONS

The Buckhorn Conglomerate and Poison Strip Sandstone were deposited as a sinuous, single-thread DFS with downstream (west to east) decreasing channel-body amalgamation, lateral channel migration, grain size, sinuosity, and net-to-gross. This DFS ends or merges with a northward-flowing axial system (Burro Canyon Formation) near the eastern edge of Utah. Fluvial channel deposits are arranged in stacked and laterally adjacent point-bar deposits of multistory and multilateral architectures with isolated channels limited to the distal parts of the DFS. The fluvial system drained a 10^6 km^2-scale area. The meandering planform persisted down depositional dip (west-east) and through time (vertically), challenging the interpretation of a braided-river origin.

ACKNOWLEDGMENTS

This work was funded by the SAFARI group. We are deeply grateful to Joe Phillips, Sean Kelly, James Mullins, Ryan King, and Jostein Myking Kjærefjord for help in the field.

REFERENCES

Allen, J.R.L., 1983, Studies in fluviatile sedimentation: Bars, bar complexes and sandstone sheets (low sinuosity braided streams) in the Brownstones (L. Devonian), Welsh Borders: Sedimentary Geology, v. 33, p. 237–293.

Allmendinger, R.W., 2020, Stereonet 10, Program for stereographic projection.

Armstrong, R.L., 1968, Sevier orogenic belt in Nevada and Utah: Geological Society of America, Bulletin, v. 79, no. 4, p. 429-458.

Aubrey, W.M., 1992, New interpretations of the stratigraphy and sedimentology of uppermost Jurassic to lowermost Upper Cretaceous strata in the San Juan basin of northwestern New Mexico: U.S. Geological Survey, Bulletin 1808–J, p. J1–J17.

Ayers, J.D., 2004, Lithological evidence of the Jurassic/Cretaceous boundary within the nonmarine Cedar Mountain Formation, San Rafael Swell, Utah [Thesis]: Athens, Ohio University, 189 p.

Barclay, R.S., Rioux, M., Meyer, L.B., Bowring, S.A., Johnson, K.R., and Miller, I.M., 2015, High precision U-Pb zircon geochronology for Cenomanian Dakota Formation floras in Utah: Cretaceous Research, v. 52, p. 213-237.

Bhattacharya, J.P., and Tye, R.S., 2004, Searching for modern Ferron analogs and application to subsurface interpretation, *in* Chidsey, T.C., Jr., Adams, R.D., and Morris, T.H., eds., The Fluvial-Deltaic Ferron Sandstone: Regional to Wellbore-Scale Outcrop Analog Studies and Application to Reservoir Modeling: American Association of Petroleum Geologists, Studies in Geology v. 50, p. 39–57.

Bhattacharya, J.P., and MacEachern, J.A., 2009, Hyperpycnal Rivers and Prodeltaic Shelves in the Cretaceous Seaway of North America: Journal of Sedimentary Research, v. 79, p. 184–209.

Bhattacharyya, P., Bhattacharya, J.P., Khan, S.D., 2015, Paleo-Channel Reconstruction and Grain Size Variability in Fluvial Deposits, Ferron Sandstone, Notom Delta, Hanksville Utah: Sedimentary Geology v. 325, p. 17–25.

Bhattacharya, J.P., Copeland, P., Lawton, T.F., and Holbrook, J., 2016, Estimation of source area, river paleo-discharge, paleoslope, and sediment budgets of linked deep-time depositional systems and implications for hydrocarbon potential: Earth-Science Reviews, v. 153, p. 77-110.

Blum, M., Martin, J., Milliken, K., and Garvin, M., 2013, Paleovalley systems: insights from Quaternary analogs and experiments: Earth-Science Reviews, v. 116, p. 128–169.

Blum, M., and Pecha, M., 2014, Mid-Cretaceous to Paleocene North American drainage reorganization from detrital zircons: Geology, v. 42, p. 607–610.

Bookhagen, B., and Burbank, D.W., 2010, Toward a complete Himalayan hydrological budget: Spatiotemporal distribution of snowmelt and rainfall and their impact on river discharge: Journal of Geophysical Research, v. 115, p. 1-25.

Brice, J.C., 1982, Stream-channel stability assessment: Federal Highway Administration Report No. FHWA/RD-82/021, Washington, DC, 42 p.

Bridge, J.S., and Mackey, S.D., 1993, A theoretical study of fluvial sandstone body dimensions, *in* Flint, S.S., and Bryant, I.D., eds., Geological modeling of hydrocarbon reservoirs: International Association of Sedimentologists, Special Publication 15, p. 213-236.

Bridge, J.S., 2006, Fluvial facies models: recent developments, *in* Posamentier, H.W., and Walker, R.G., eds., Facies Models Revisited: SEPM, Special Publication 84, p. 85–170.

Braudrick, C.A., 2013, Meandering in gravel-bed rivers, [Dissertation]: University of California, Berkeley, 220 p.

Buckley, S.J., Howell, J.A., Enge, H.D., and Kurz, T.H., 2008, Terrestrial laser scanning in geology: data acquisition, processing and accuracy considerations, Geological Society of London, Journal, v. 165, p. 625-638.

Buckley, S.J., Ringdal, K., Naumann, N., Dolva, B., Kurz, T.H., Howell, J.A., and Dewez, T.J.B., 2019, LIME: Software for 3-D visualization, interpretation, and communication of virtual geoscience models, Geosphere, 15(1).

Burton, D., Greenhalgh, B.W., Britt, B.B., Kowallis, B.J., Elliott, W.S., and Barrick, R., 2006, New radiometric ages from the Cedar Mountain Formation, Utah and the Cloverly Formation, Wyoming: implications for contained dinosaur faunas: Geological Society of America, Abstracts with Programs, v. 38, 52 p.

Cant, D.J., 1982, Fluvial facies models and their application, *in* Scholle, P.A., and Spearing, D., eds., Sandstone Depositional Environments: American Association of Petroleum Geologists, Memoir 31, p. 115–137.

Cardenas, B.T., Mohrig, D., Goudge, T.A., Hughes, C.M., Levy, J.S., Swanson, T., Mason, J., and Zhao, F., 2020, The anatomy of exhumed river-channel belts: Bedform to belt-scale river kinematics of the Ruby Ranch Member, Cretaceous Cedar Mountain Formation, Utah, USA: Sedimentology, v. 67, p. 3655–3682.

Cifelli, R.L., Kirkland, J.I., Weil, A., Deino, A.L., and Kowallis, B.J., 1997, High-precision ^{40}Ar/^{39}Ar geochronology and the advent of North America’s Late Cretaceous terrestrial fauna: Proceedings of the National Academy of Sciences (USA), v. 94, no. 21, p. 11,163-11,167.

Clayton, J.A., and Pitlick, J., 2007, Spatial and temporal variations in bed load transport intensity in a gravel bed river bend, Water Resources Research, v. 43, p. 1-13.

Cobban, W.A., Walaszczyk, I., Obradovich, J.D., and McKinney, K.C., 2006, A USGS zonal table for the Upper Cretaceous Middle Cenomanian−Maastrichtian of the Western Interior of the United States based on ammonites, inoceramids, and radiometric ages: US Geological Survey, Open File Report, v. 2006–1250, 50 p.

Conley, S.J., 1986, Stratigraphy and depositional environment of the Buckhorn Conglomerate Member of the Cedar Mountain Formation (Lower Cretaceous), central Utah [Thesis]: Fort Hays State University, 174 p.

Craig, L.C., 1981, Lower Cretaceous rocks, southwestern Colorado and southeastern Utah, *in* Wiegand, D.L., ed., Geology of the Paradox basin: Rocky Mountain Association of Geologists Guidebook, 1981 Field Conference, p. 195-200.

Crane, R.C., 1982, A computer model for the architecture of avulsion controlled alluvial suites: [Thesis]: University of Reading, 534 p.

Currie, B.S., 1997, Sequence stratigraphy of nonmarine Jurassic-Cretaceous rocks, central Cordilleran foreland-basin system: Geological Society of America, Bulletin, v. 109, no. 9, p. 1206-1222.

Currie, B.S., 1998, Upper Jurassic–Lower Cretaceous Morrison and Cedar Mountain Formations, NE Utah–NW Colorado: relationships between nonmarine deposition and early Cordilleran foreland basin development: Journal of Sedimentary Research, v. 68, p. 632–652.

Currie, B.S., 2002, Structural configuration of the Early Cretaceous Cordilleran foreland-basin system and Sevier Thrust Belt, Utah and Colorado: The Journal of Geology, v. 110, no. 6, p. 697-718.

Davidson, S.K., and Hartley, A.J., 2010, A quantitative approach to linking drainage area with distributive fluvial system area in dryland, endorheic basin settings: Geomorphology v. 180, p. 82–95.

Davidson, S.K., Hartley, A.J., Weissmann, G.S., Nichols, G.J., and Scuderi, L.A., 2013, Geomorphic elements on modern distributive fluvial systems: Geomorphology, v. 180-181, p. 82–95.

DeCelles, P.G., and Currie, B.S., 1996, Long-term sediment accumulation in the Middle Jurassic-early Eocene Cordilleran retroarc foreland-basin system: Geology, v. 24, p. 591–594.

DeCelles, P.G., and Giles, K.N., 1996, Foreland basin systems: Basin Research, v. 8, p. 105–123.

DeCelles, P.G., 2004, Late Jurassic to Eocene evolution of the Cordilleran thrust belt and foreland basin system, western U.S.A.: American Journal of Science, v. 304, p. 105-168.

Dickinson, W.R., and Gehrels, G.E., 2008, Sediment delivery to the Cordilleran foreland basin: Insights from U-Pb ages of detrital zircons in Upper Jurassic and Cretaceous strata of the Colorado Plateau: American Journal of Science, v. 308, p. 1041–1082.

Ethridge, F.G., 2011, Interpretation of ancient fluvial channel deposits: review and recommendations, *in* Stephanie, K., Davidson, S.K., Leleu, S., and North, C.P., eds., From River to Rock Record: SEPM, Special Publication 97, p. 9–35.

Fabuel-Perez, I., Hodgetts, D., and Redfern, J., 2009, A new approach for outcrop characterization and geostatistical analysis of a low-sinuosity fluvial-dominated succession using digital outcrop models: Upper Triassic Oukaimeden Sandstone Formation, central high Atlas, Morocco: American Association of Petroleum Geologists, Bulletin, v. 93, p. 795–827.

Garrison, J.R., Brinkman, D., Nichols, D.J., Layer, P., Burge, D., and Thayn, D., 2007, A multidisciplinary study of the Lower Cretaceous Cedar Mountain Formation, Mussentuchit Wash, Utah: a determination of the paleoenvironment and paleoecology of the *Eolambia caroljonesa* dinosaur quarry: Cretaceous Research, v. 28, no. 3, p. 461-494.

Ghinassi, M., Billi, P., Libsekal, Y., Papini, M. and Rook, L., 2013, Inferring fluvial morphodynamics and overbank flow control from 3D outcrop sections of a Pleistocene point bar, Dandiero Basin, Eritrea: Journal of Sedimentary Research, v. 83, p. 1066–1084.

Ghinassi, M., Nemec, W., Aldinucci, M., Nehyba, S., Özaksoy, V. and Fidolini, F., 2014, Planform evolution of ancient meandering rivers reconstructed from longitudinal outcrop sections: Sedimentology, v. 61, p. 952–977.

Ghinassi, M., and Ielpi, A., 2015, Stratal architecture and morphodynamics of downstream migrating fluvial point bars (Jurassic Scalby Formation, UK): Journal of Sedimentary Research, v. 85, p. 1123–1137.

Greenhalgh, B.W., 2006, A stratigraphic and geochronologic analysis of the Morrison Formation/Cedar Mountain Formation boundary, Utah [Thesis]: Provo, Utah, Brigham Young University, 61 p.

Gupta, S., 1997, Himalayan drainage patterns and the origin of fluvial megafans in the Ganges foreland basin: Geology, v. 25, p. 11-14.

Hartley, A.J., Weissmann, G.S., Nichols, G.J., and Warwick, G.L., 2010, Large distributive fluvial systems: characteristics, distribution, and controls on development: Journal of Sedimentary Research, v. 80, p. 167–183.

Hartley, A.J., Owen, A.E., Swan, A., Weissmann, G.S., Holzweber, B.I., Howell, J., Nichols, G.D., and Scuderi, L.A., 2015, Recognition and importance of amalgamated sandy meander belts in the continental rock record: Geology v. 43, p. 679–682.

Heller, P.L., and Paola, C., 1989, The paradox of Lower Cretaceous gravels and the initiation of thrusting in the Sevier orogenic belt, United States western interior: Geological Society of America, Bulletin, v. 101, p. 864–875.

Heller, P.L., Duecker, K., and McMillan, M.E., 2003, Post-Paleozoic alluvial gravel transport as evidence of continental tilting in the U.S. Cordillera: Geological Society of America, Bulletin, v. 115, p. 1122–1132.

Hendrix, B., Möller, A., Ludvigson, G.A., Joeckel, R.M., and Kirkland, J.I., 2015, A new approach to date paleosols in terrestrial strata: A case study using U-Pb zircon ages for the Yellow Cat Member of the Cedar Mountain Formation of eastern Utah: Geological Society of America, Abstracts with Programs, v. 47, p. 597.

Holmes, A.D., 2017, Sedimentology and taphonomy of the *Abydosaurus mcintoshi* quarry, (Naturita Formation, Early Cretaceous, Latest Albian), Dinosaur National Monument, Utah [MS Thesis]: Brigham Young University, Provo, Utah, 60 p.

Horton B.K., and DeCelles P.G., 2001, Modern and ancient fluvial megafans in the foreland basin system of the central Andes, southern Bolivia: Implications for drainage network evolution in fold-thrust belts: Basin Research, v. 13, p. 43–63.

Hunt, G.J., Lawton, T.F., and Kirkland, J.I., 2011, Detrital zircon U-Pb geochronological provenance of Lower Cretaceous strata, foreland basin, Utah, *in* Sprinkel, D.A., Yonkee, W.A., and Chidsey, T.C., Jr., eds., Sevier Thrust Belt—Northern and Central Utah and Adjacent Areas: Utah Geological Association, Publication 40, p. 193–211.

Ielpi, A., and Ghinassi, M., 2014, Planform architecture, stratigraphic signature and morphodynamics of an exhumed Jurassic meander plain (Scalby Formation, Yorkshire, UK): Sedimentology, v. 61, p. 1923–1960.

Joeckel, R.M., Ludvigson, G.A., and Kirkland, J.I. 2017, Lower Cretaceous paleo-Vertisols and sedimentary interrelationships in stacked alluvial sequences, Utah, USA: Sedimentary Geology, v. 361, p. 1–24.

Joeckel, R.M., Ludvigson, G.A., Möller, A., Hotton, C.L., Suarez, M.B., Suarez, C.A., Sames, B., Kirkland, J.I., and Hendrix, B., 2019, Chronostratigraphy and terrestrial palaeoclimatology of Berriasian–Hauterivian strata of the Cedar Mountain Formation, Utah, USA, *in* Wagreich, M., Hart, M.B., Sames, B., and Yilmaz, I.O., eds., Cretaceous Climate Events and Short-term Sea-level Changes: Geological Society of London, Special Publication 498, p. 75-100.

Kirkland, J.I., Britt, B.B., Burge, D.L., Carpenter, K., Cifelli, R.L., DeCourten, F.L., Eaton, J.G., Hasiotis, S.T., and Lawton, T.F., 1997, Lower to middle Cretaceous dinosaur faunas of the central Colorado Plateau: a key to understanding 35 million years of tectonics, sedimentology, evolution and biogeography: Brigham Young University, Geology Studies, v. 42, no. 2, p. 69-103.

Kirkland, J.I., and Madsen, S.K., 2007, The Lower Cretaceous Cedar Mountain Formation, eastern Utah—the view up an always interesting learning curve, *in* Lund, W.R., ed., Field Guide to Geological Excursions in Southern Utah: Geological Society of America, Rocky Mountain Section, 2007 Annual Meeting, Grand Junction Geological Society and Utah Geological Association Publication 35, p. 1–108, compact disk.

Kirkland, J.I., Suarez, M., Suarez, C., and Hunt-Foster, R., 2016, The Lower Cretaceous in east-central Utah – the Cedar Mountain Formation and its bounding strata: Utah Geological Association, Geology of the Intermountain West, v.3, Field Trip Guide, Society of Vertebrate Paleontology, Salt Lake City, Utah, October 26–29, 130 p.

Kirkland, J.I., 2017, Does Utah preserve North America's oldest Cretaceous dinosaurs because of ancient salt deposits? Utah Geological Survey, Survey Notes, v. 49, p. 4-5.

Lawton, T.F., Sprinkel, D.A., DeCelles, P.G., Mitra, G., Sussman, A.J., and Weiss, M.P., 1997, Stratigraphy and structure of the Sevier thrust belt and proximal foreland-basin system in central Utah: A transect from the Sevier Desert to the Wasatch Plateau: Brigham Young University, Geology Studies, v. 42, p. 33-67.

Lawton, T.F., Hunt, G.J., and Gehrels, G.E., 2010, Detrital zircon record of thrust belt unroofing in Lower Cretaceous synorogenic conglomerates, central Utah: Geology, v. 38, p. 463–466.

Ludvigson, G.A., Joeckel, R.M., Gonzalez, L.A., Gulbranson, E.L., and Rasbury, E.T., 2010, Correlation of Aptian-Albian carbon isotope excursions in continental strata of the Cretaceous foreland basin, eastern Utah, U.S.A.: Journal of Sedimentary Research, v. 80, p. 955–74.

Ludvigson, G.A., Joeckel, R.M., Murphy, L.R., Stockli, D.F., González, L.A., Suarez, C.A., Kirkland, J.I., and Al-Suwaidi, A., 2015, The emerging terrestrial record of Aptian-Albian global change: Cretaceous Research, v. 56, p. 1–24.

Lunt, L.A., and Bridge, J.S., 2004, Evolution and deposits of a gravelly braid bar, Sagavanirktok River, Alaska: Sedimentology, v. 51, p. 415–432.

Matthai, H.F., 1990, Floods: Surface Water Hydrology: Geological Society of America, v. 1, p. 97–120.

Métivier, F., and Barrier, L., 2012, Chapter 34: Alluvial landscape evolution: what do we know about metamorphosis of gravel-bed meandering and braided streams?, *in* Church, M., Biron, P.M., and Roy, A.G., eds., Gravel-Bed Rivers: Processes, Tools, Environments: Wiley-Blackwell, p. 474-501.

Miall, A.D., 1977, A review of the braided river depositional environment: Earth-Science Reviews, v. 13, p. 1–62.

Miall, A.D., 2010, Alluvial Deposits, *in*, James, N.P., and Dalrymple, R.W., eds., Facies Models, 4th Edition: Geological Association of Canada, p. 105-137.

Montgomery, E.H., Suarez, M., Gray, W., Kirkland, J.I., Suarez, C., and Al-Suwaidi, A., 2013, Organic carbon chemostratigraphy and x-ray diffraction (XRD) mineralogy in lacustrine strata of the Ruby Ranch Member within the Cedar Mountain Formation near Moab, Utah: Geological Society of America, Abstracts with Programs, v. 45, no. 7, p. 619.

Mori, H., 2009, Dinosaurian faunas of the Cedar Mountain Formation and LA-ICP-MS detrital zircon ages for three stratigraphic sections [Thesis]: Bigham Young University, Provo, Utah, 108 p.

Mulder, T., and Syvitski, J.P., 1995, Turbidity currents generated at river mouths during exceptional discharges to the world oceans: Journal of Geology, v. 103, no. 3, p. 285-299.

Owen, A., Nichols, G.J., Hartley, A.J., Weissmann, G.S., and Scuderi, L.A., 2015, Quantification of a distributive fluvial system: The Salt Wash DFS of the Morrison Formation, SW USA: Journal of Sedimentary Research, v. 85, p. 544–561.

Owen, A., Hartley, A.J., Ebinghaus, A., Weissmann, G.S., and Santos, M.G.M., 2019, Basin-scale predictive models of alluvial architecture: Constraints from the Palaeocene–Eocene, Bighorn Basin, Wyoming, USA: Sedimentology, v. 66, p. 736–763.

Phillips, S.P., Howell, J.A., Hartley, A.J., Chmielewska, M., and Hudson, S.M., 2021, Evolution of foreland basin fluvial systems in the mid-Cretaceous of Utah, USA (upper Cedar Mountain and Naturita formations): Sedimentology, v. 68, no. 5, p. 2097–2124.

Primm, J., Johnson, C., and Stearns, M., 2018, Basin-axial progradation of a sediment supply-driven distributive fluvial system in the Late Cretaceous southern Utah foreland: Basin Research, v. 30, p. 249–278.

Rittersbacher, A., Howell, J.A., and Buckley, S.J., 2014, Analysis of fluvial architecture in the Blackhawk Formation, Wasatch Plateau, Utah, U.S.A., using large 3D photorealistic models: Journal of Sedimentary Research, v. 84, p. 72–87.

Roca, X.A., 2003, Tectonic and sequence stratigraphic implications of the Morrison Formation, Buckhorn Conglomerate transition, Cedar Mountain, east-central Utah [Thesis]: Athens, Ohio University, 222 p.

Roca, X., and Nadon, G.C., 2007, Tectonic control on the sequence stratigraphy of nonmarine retroarc foreland basin fills—insights from the Upper Jurassic of central Utah, U.S.A.: Journal of Sedimentary Geology, v. 77, p. 233–255.

Royse, F., 1993, Case of the phantom foredeep: Early Cretaceous in west-central Utah: Geology, v. 21, p. 133–136.

Rubin, D.M., and McCulloch, D.S., 1980, Single and superimposed bedforms: a synthesis of San Francisco Bay and flume observations: Sedimentary Geology, v. 26, p. 207–231.

Shukla, U.K., Singh, I.B., Sharma, M., and Sharma, S., 2001, A model of alluvial megafan sedimentation: Ganga Megafan: Sedimentary Geology, v. 144, p. 243 – 262.

Stikes, M.W., 2007, Fluvial facies and architecture of the Poison Strip Sandstone, Lower Cretaceous Cedar Mountain Formation, Grand County, Utah: Utah Geological Survey, Miscellaneous Publication 06-2, 84 p., compact disc.

Stokes, W.L., 1944, Morrison formation and related deposits in and adjacent to the Colorado Plateau: Geological Society of America, Bulletin, v. 55, no. 8, p. 951-992.

Stokes, W.L., 1952, Lower Cretaceous in Colorado Plateau: American Association of Petroleum Geologists, Bulletin, v. 36, p. 1766–1776.

Swan, A., Hartley, A.J., Owen, A., and Howell, J., 2018, Reconstruction of a sandy point-bar deposit: implications for fluvial facies analysis, *in* Ghinassi, M., Colombera, L., Mountney, N.P., Reesink, A.J.H., and Bateman, M., eds., Fluvial Meanders and Their Sedimentary Products in the Rock Record: International Association of Sedimentologists, Special Publication 48, p. 445–474.

Trujillo, K.C., and Kowallis, B.J., 2015, Recalibrated legacy ^{40}Ar/^{39}Ar ages for the Upper Jurassic Morrison Formation, Western Interior, U.S.A.: Geology of the Intermountain West, v. 2, p. 1–8.

Tucker, R.T., Zanno, L.E., Huang, H.-Q., Makovicky, P.J., 2020, A refined temporal framework for newly discovered fossil assemblages of the upper Cedar Mountain Formation (Mussentuchit Member), Mussentuchit Wash, Central Utah: Cretaceous Research, v. 110, 23 p.

Valenza, J.M., Edmonds, D.A., Hwang, T., and Roy, S., 2020, Downstream changes in river avulsion style are related to channel morphology, Nature Communications, v. 11, p. 1-8.

Weissmann, G.S., Hartley, A.J., Nichols, G.J., Scuderi, L.A., Olson, M.E., Buehler, H., and Banteah, R., 2010, Fluvial form in modern continental sedimentary basins: distributive fluvial systems: Geology, v. 38, p. 39–42.

Weissmann, G.S., Hartley, A.J., Scuderi, L.A., Nichols, G.J., Davidson, S.K., Owen, A., Atchley, S.C., Bhattacharyya, P., Ghosh, P., Nordt, L.C., Michel, L. and Tabor, N.J., 2013, Prograding distributive fluvial systems - geomorphic models and ancient examples, in Dreise, S.G., Nordt, L.C., and McCarthy, P.L., eds., New Frontiers in Paleopedology and Terrestrial Paleoclimatology: SEPM, Special Publication 104, p. 131–147.

Weissmann, G.S., Hartley, A.J., Scuderi, L.A., Nichols, G.J., Owen, A., Wright, S., Felicia, A.L., Holland, F., and Anaya, F.M.L., 2015, Fluvial geomorphic elements in modern sedimentary basins and their potential preservation in the rock record: a review: Geomorphology, v. 250, p. 187–219.

Yingling, V.L., 1987, Timing and initiation of Sevier orogeny: Morrison and Cedar Mountain Formations and Dakota Sandstone, east-central Utah [Thesis]: University of Wyoming, Laramie, 169 p.

Young, R.G., 1973, Depositional environments of basal Cretaceous rocks of the Colorado Plateau, *in* Fassett, J.E., ed., Cretaceous and Tertiary Rocks of the Southern Colorado Plateau: A Memoir of the Four Corners Geological Society: Four Corners Geological Society, p. 10-27.

FIGURES AND CAPTIONS

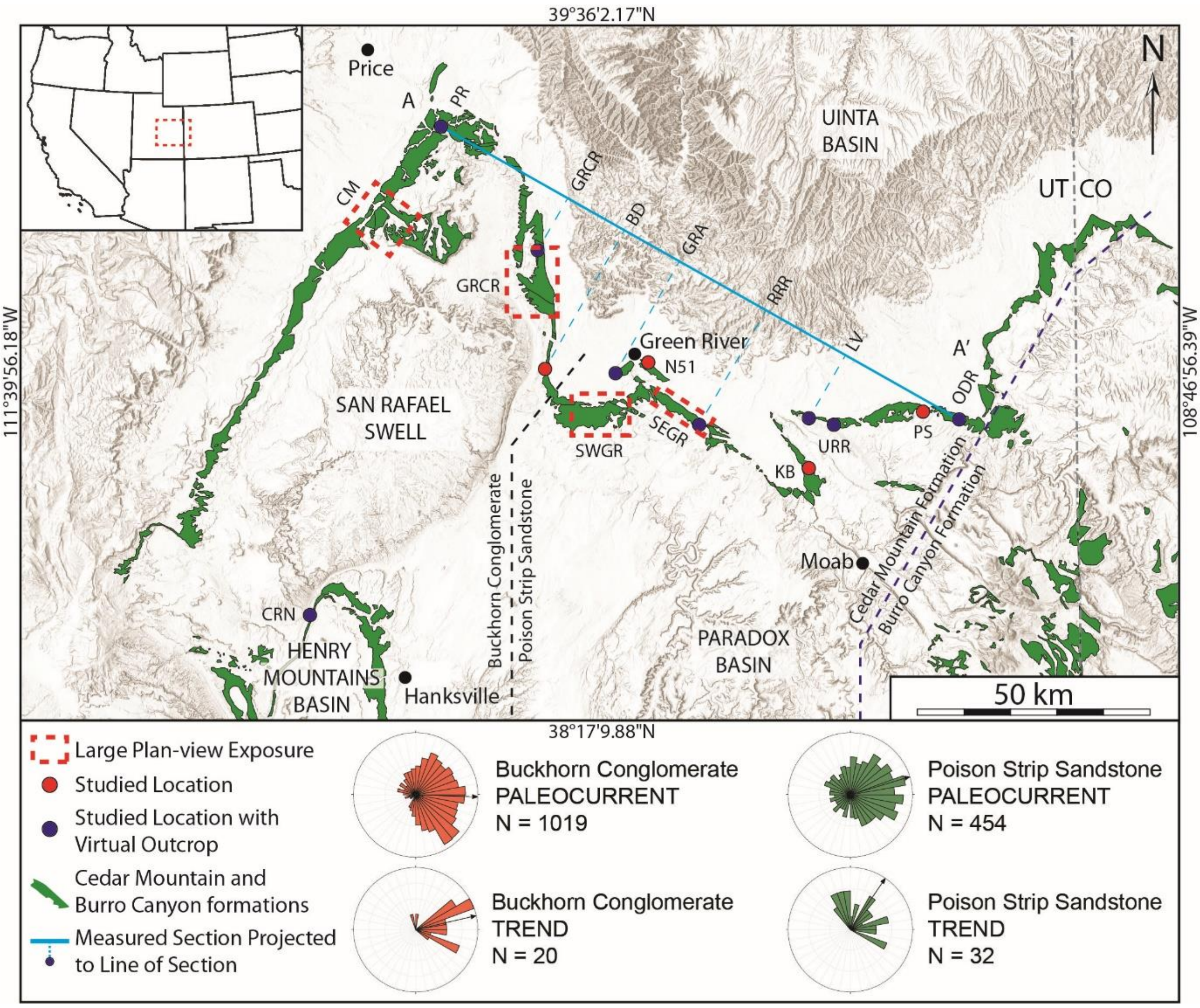

Figure 1: Map of the study area. Studied locations are shown superimposed on mapped outcrop of the Early Cretaceous. Line of section A-A' refers to Figure 3. Paleocurrent measurements from cross-bedding and measurements of the trend of channel axes are reported indicating an eastern paleocurrent direction for the Buckhorn Conglomerate and a northeastern paleocurrent direction for the Poison Strip Sandstone. Abbreviations: CM = Cedar Mountain, PR = Price River, GRCR = Green River Cutoff Road, BD = Buckmaster Draw, GRA = Green River Airport, SWGR = Southwest Green River, SEGR = Southeast Green River, N51 = New Area 51, RRR = Ruby Ranch Road, LV = Long Valley, KB = Klondike Bluffs, URR = Utahraptor Ridge, PS = Poison Strip, ODR = Owl Draw Road, CRN = Caineville Reef North.

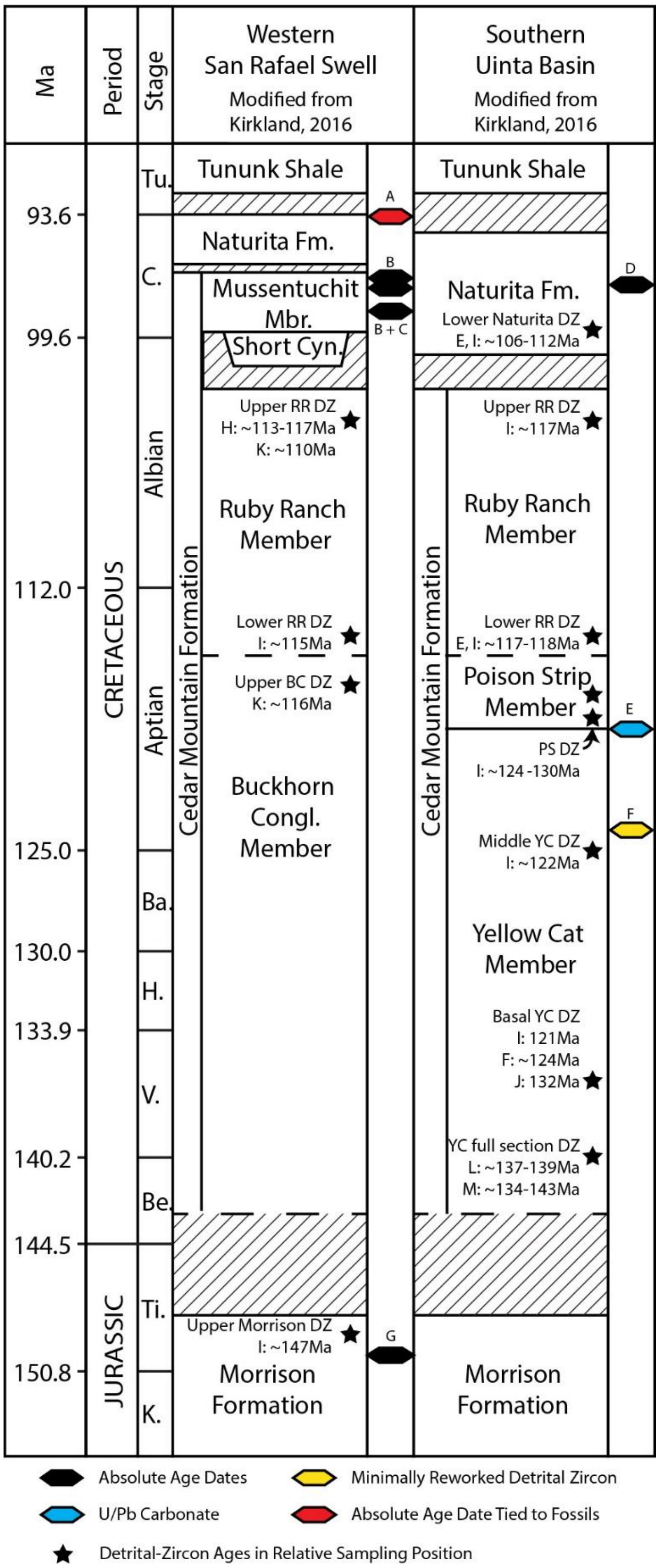

Figure 2: Stratigraphic columns with absolute and detrital-zircon ages. Absolute ages are matched to the time scale at left. Detrital ages are indicated in their relative sampling position in the stratigraphic column. A) Cobban et al., 2006; B) Garrison et al., 2007; C) Cifelli et al., 1997; D) Barclay

et al., 2015; E) Ludvigson et al., 2010; F) Greenhalgh, 2006; G) Trujillo and Kowallis, 2015; H) Burton et al., 2006; I) Mori, 2009; J) Kirkland et al., 2016; K) Tucker et al., 2020; L) Hendrix et al., 2015; M) Joeckel et al., 2019.

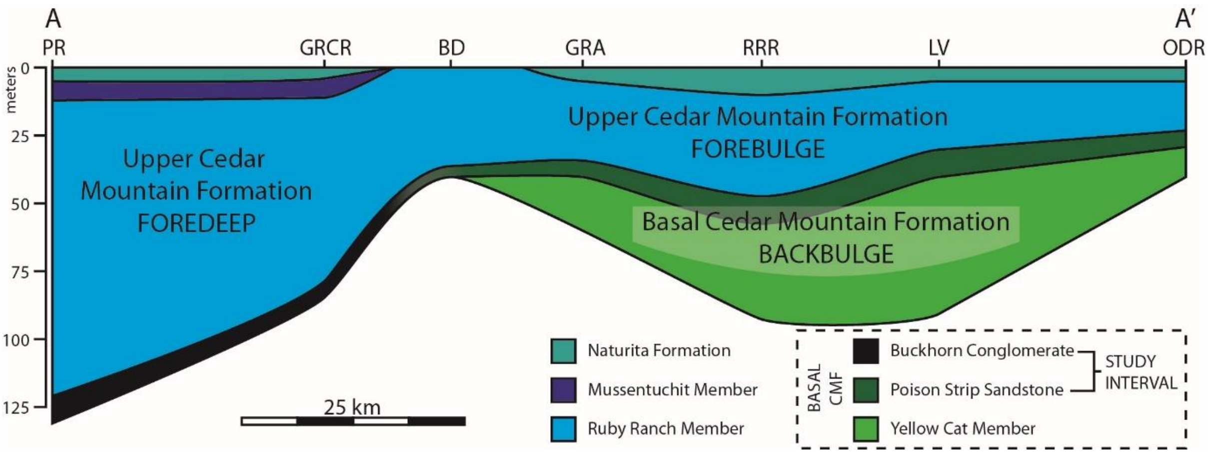

Figure 3: Crosssection that shows the foredeep to forebulge thinning geometry of upper Cedar Mountain Formation deposits and the eastward thickening of deposits of the study interval. See Figure 1 for abbreviation definitions.

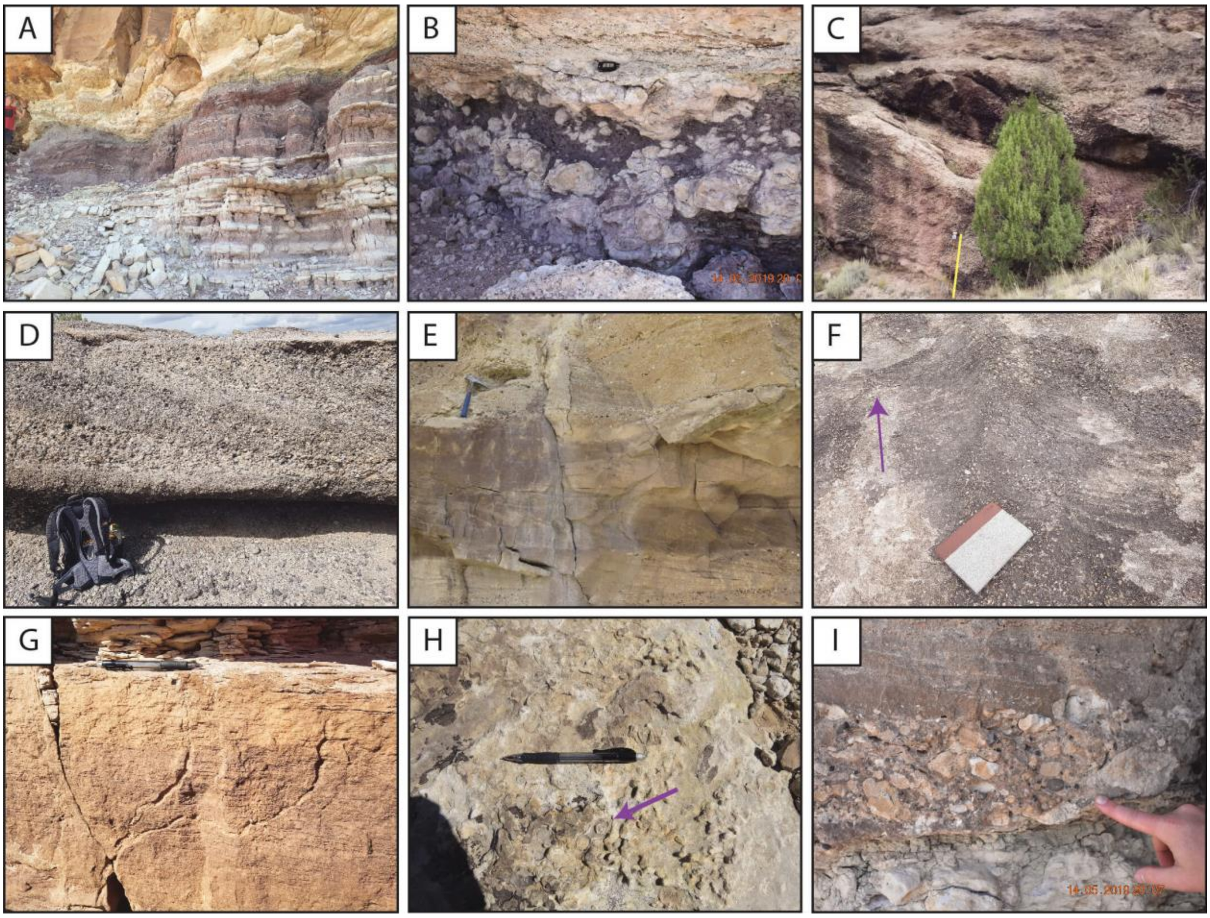

Figure 4: Common facies in the study interval. A) Mudstone and thin splay deposits beneath a channel body of the Poison Strip Sandstone. B) Well-developed caliche underneath channel deposits. C) Meter-scale trough cross-stratified extrabasinal conglomerate of pebble to cobble size. Jacob's staff is 1.5 m and highlighted with yellow line. D) Poorly sorted trough cross-stratified conglomerate of granule to pebble size. E) Trough cross-stratified sandstone with trough cross-stratified conglomerate above and below. F) Plan-view of trough cross-stratified conglomerate. Arrow indicates flow direction. G) Ripple cross-stratified sandstone with burrows. Ripples are quite low-profile making parts of this outcrop appear planar laminated. H) Rooted sandstone. Note the concentric rings within root traces. I) Basal lag composed of intrabasinal and extrabasinal clasts. Intrabasinal clasts are caliche nodules sourced from caliche beds below and adjacent to channel deposits.

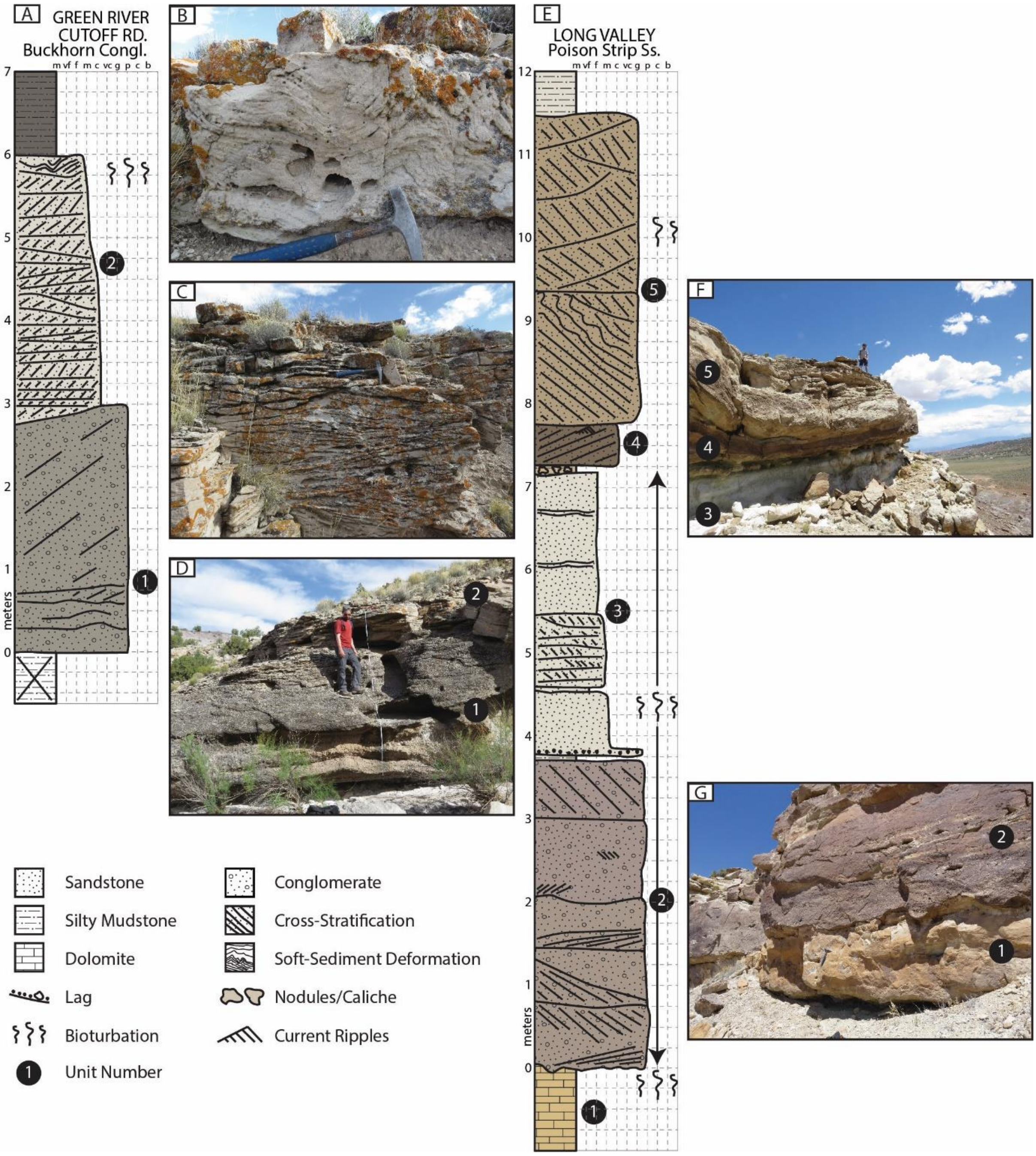

Figure 5: Representative stratigraphic logs for the Buckhorn Conglomerate and Poison Strip Sandstone. A) Stratigraphic log through the Buckhorn Conglomerate from the Green River Cutoff Road. Numbers are shown to match the log to the outcrop photo in part D. Location: 39°11'49.80" N, 110°22'42.33" W. B) Soft-sediment deformation in the upper part of “unit 2”. C) Cross-stratification in “unit 2”. D) Photograph of the outcrop showing the different “units”. Numbers on the outcrop are matched to the stratigraphic log in part A. E) Stratigraphic log through the Poison Strip Member from Long Valley. Numbers are shown to match the log to the outcrop photo in parts F and G. Location:

38°51'56.75" N, 109°42'52.53" W. F) Photograph of the upper part of the logged outcrop. G) Photograph of the lower part of the logged outcrop. Numbers on the outcrop are matched to the stratigraphic log in part E.

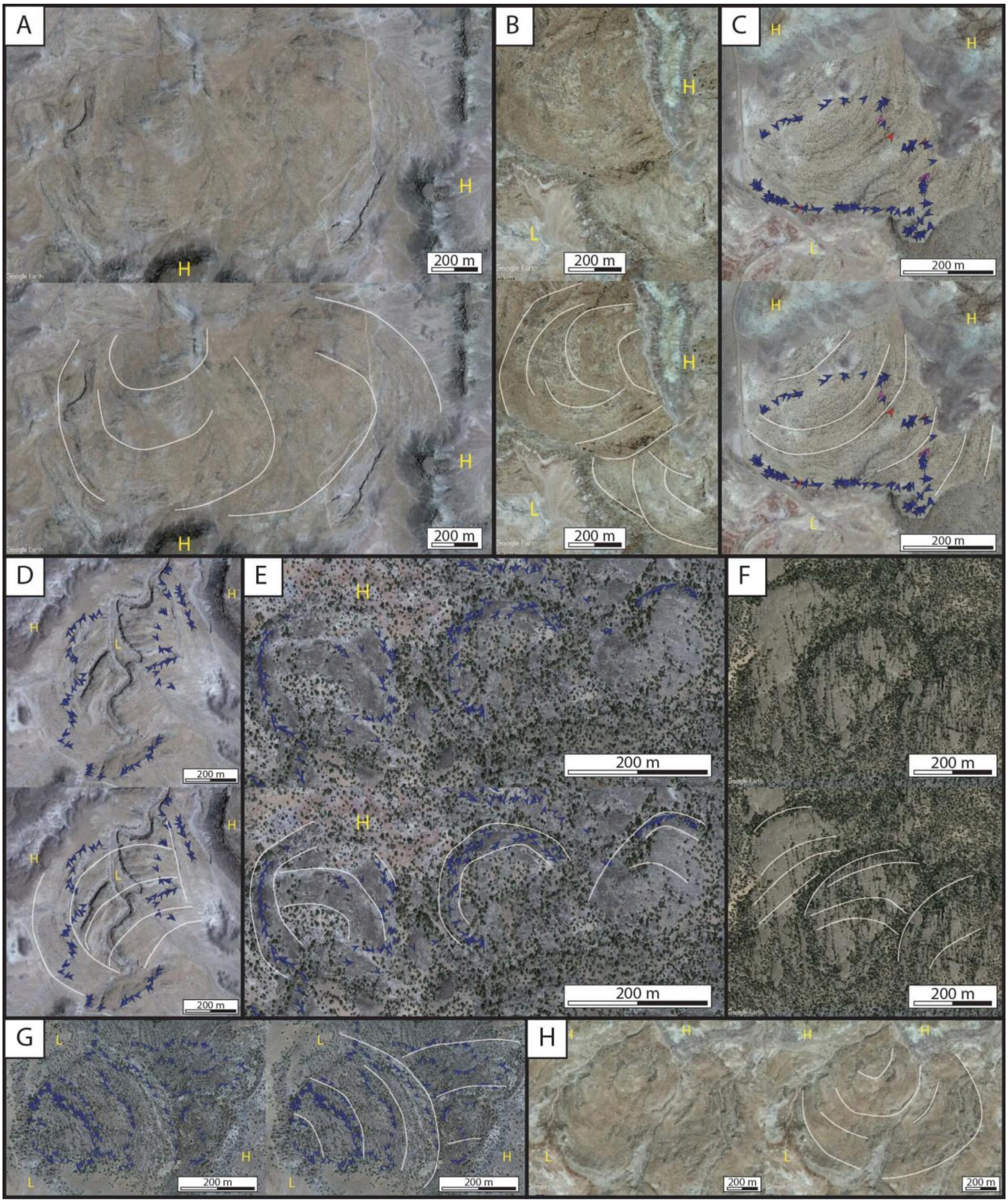

Figure 6: Plan-view examples of point-bar deposits on the upper exposure of the Buckhorn Conglomerate (BC) and the Poison Strip Sandstone (PSS). Topographic highs are denoted with an

“H”, and topographic lows are denoted with an “L”. Accretion surfaces are highlighted in white, and paleocurrent direction is indicated by small arrows. North is to the top of the page for all images. For comparison, all scale bars indicate 200 m. A) PSS. Note the lateral and downstream translation. 38°51'40.60" N, 110°17'8.57" W. B) Stacked point-bar elements, PSS. 38°52'46.23" N, 110° 2'32.73" W. C) PSS. Note that paleocurrent directions are parallel to the trend of accretion surfaces. 38°57'45.26" N, 110° 7'16.04" W. D) PSS. This point bar has been incised by a modern stream indicated by the “L”. Note that paleocurrent directions are parallel to the trend of accretion surfaces. 38°52'36.01" N, 110°16'43.45" W. E) BC. Three consecutive point bars. Note that paleocurrent directions are parallel to the trend of accretion surfaces. 39°15'13.36" N, 110°47'49.54" W. F) BC. Three consecutive and stacked point-bar elements. 39°15'34.72" N, 110°46'56.52" W. G) BC. Stacked point-bar elements. Note that paleocurrent directions are parallel to the trend of accretion surfaces. 39°10'28.15" N, 110°26'16.57" W. H) PSS. 38°53'31.88" N, 110° 3'55.70" W.

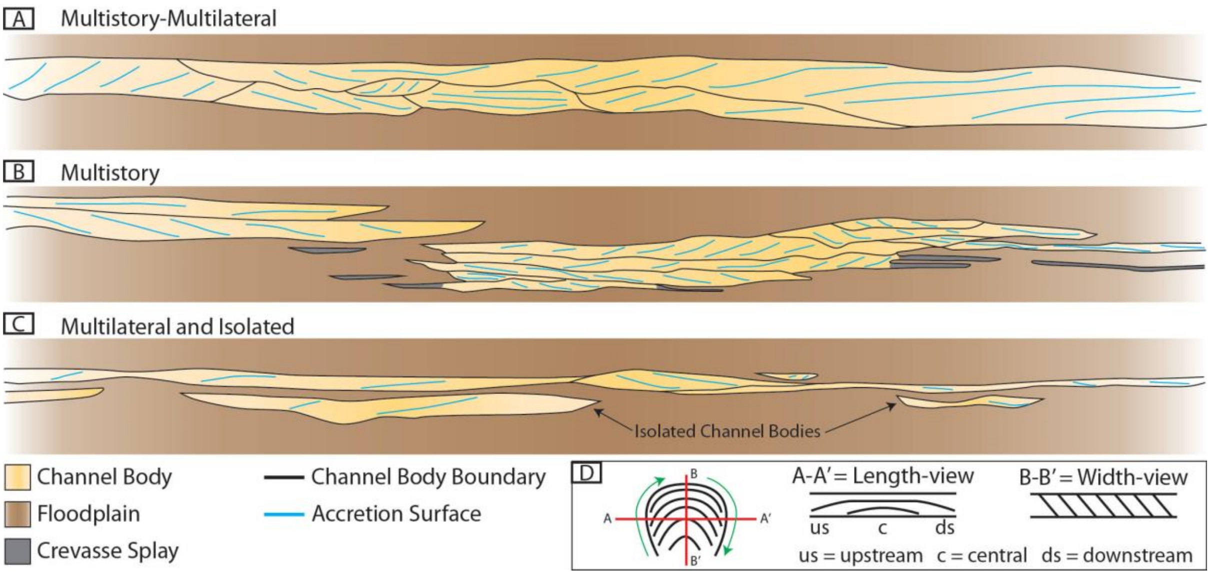

Figure 7: Architectural styles in the basal Cedar Mountain Formation. A) Multistory-multilateral deposits have a high degree of amalgamation and are common in the Buckhorn Conglomerate and Poison Strip Sandstone, but are the dominant architecture in the Buckhorn Conglomerate. B) Multistory deposits have significant vertical amalgamation and limited lateral amalgamation and are most common in the Poison Strip Sandstone. Splay deposits commonly extend laterally from these

channel bodies. C) Multilateral deposits are common in both members and display a high degree of lateral amalgamation and limited vertical amalgamation. Isolated channel bodies are limited to the Poison Strip Member. D) Definition of length and width views for subsequent architectural panels.

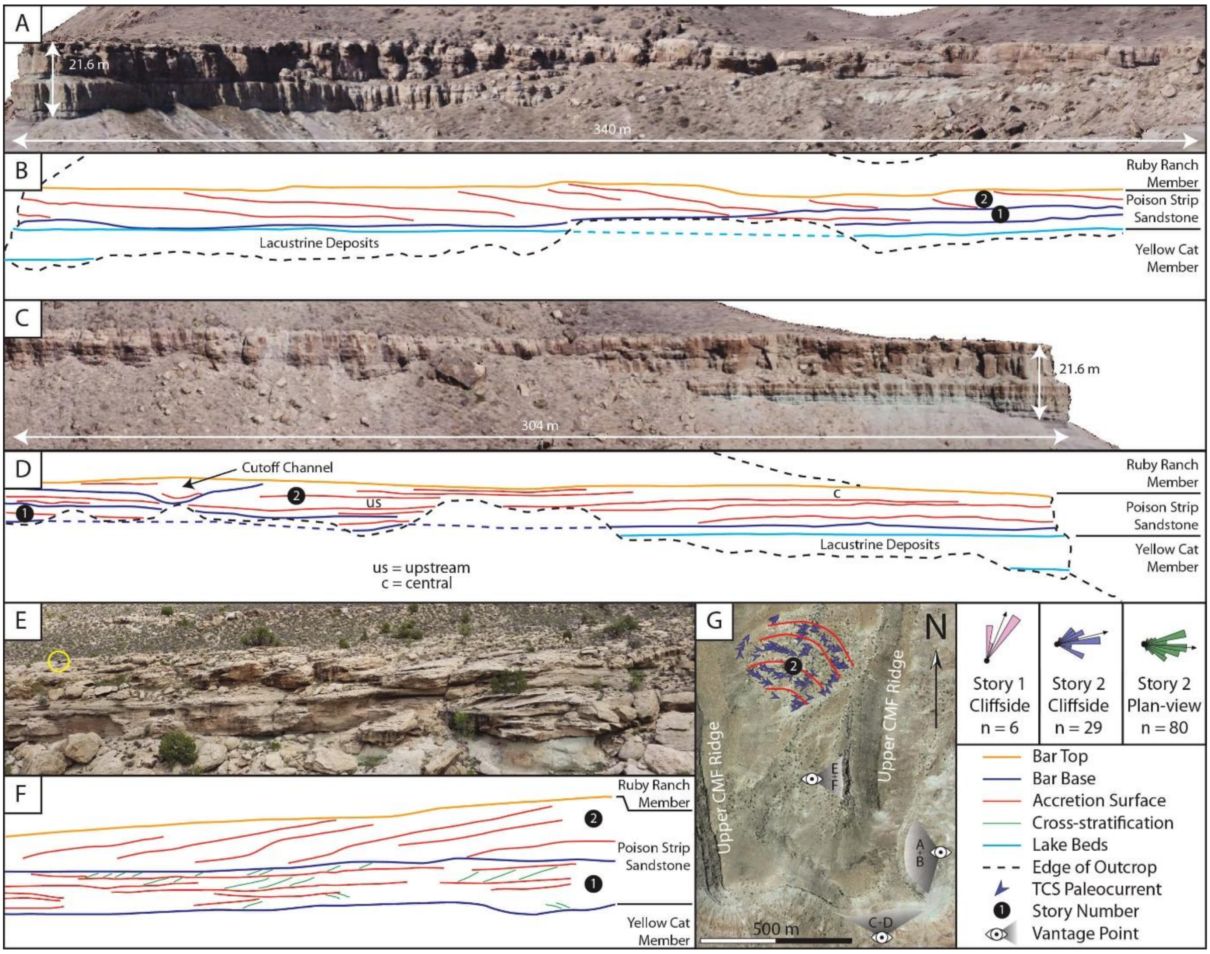

Figure 8: Architectural panels for Utahraptor Ridge. A) Orthorectified virtual outcrop of north-south-oriented cliff. B) Line drawings for part A. Note that story 1 is showing a length-view cut of a point-bar element with accretion surfaces flat to slightly concave downward, and story 2 is a width-view cut of a point-bar element showing dipping accretion surfaces from top left to bottom right. C) Orthorectified virtual outcrop of west-east-oriented cliff. D) Line drawings for part C. Note that story 1 is not prevalent on this cliff but story 2 shows a length-view cut with accretion surfaces flat to slightly concave downward. E) Photo of cliff that is parallel to part A but over the ridge to the west. Black speck circled in yellow is a backpack. Height of cliff would be similar to part A. F) Line drawings for part E. Again, note that story 1 is showing a length-view cut of a point-bar element with accretion

surfaces flat to slightly concave downward, and story 2 is a width-view cut of a point-bar element showing dipping accretion surfaces this time from top right to bottom left. G) Satellite view of the area showing vantage points for all three cliffs. Also shown are paleocurrent measurements (n = 115) for each story; both plan-view and cliff measurements are given for story 1. The plan-view exposure is between two prominent ridges capped by upper Cedar Mountain Formation channel deposits. TCS = trough cross-stratification.

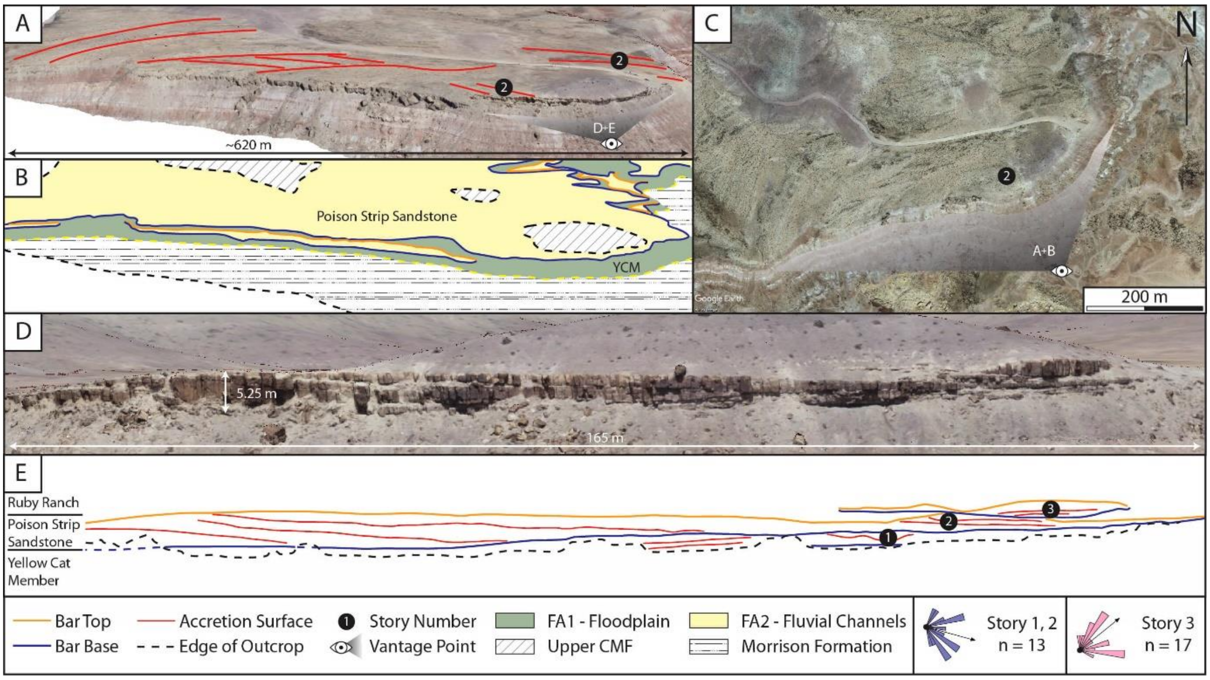

Figure 9: Architectural panels for Green River Airport (38°56'59.60" N, 110° 9'59.60" W). A) Virtual outcrop “bird’s eye” view of the Poison Strip Sandstone. Accretion surfaces are highlighted in red. Vantage point for part D is shown. B) Line drawing for part A. Note that the color fill highlights the presence of FA1 between deposits of FA2. C) Satellite view of area. Vantage point for part A is shown. D) Orthorectified virtual outcrop cliff image. E) Line drawing showing stacked bars with lateral accretion as indicated by the dipping accretion surfaces and paleocurrent data.

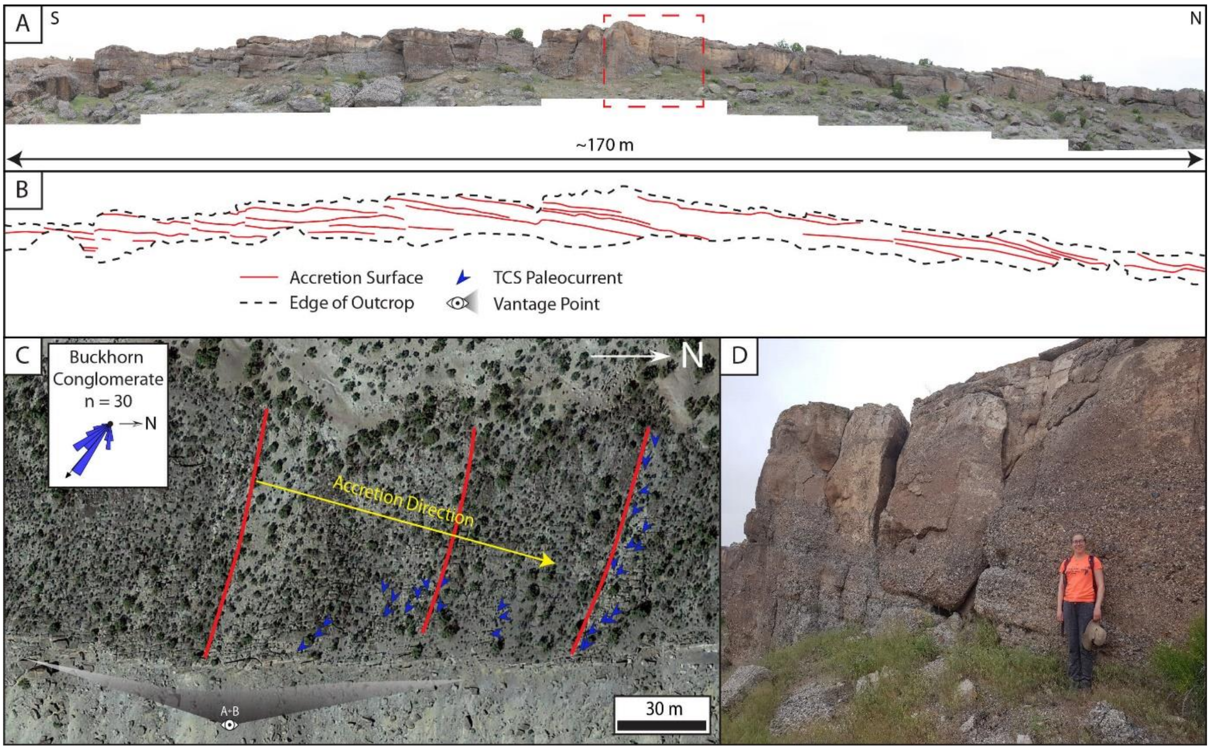

Figure 10: Buckhorn Conglomerate from the Woodside Dome (39°10'16.05" N, 110°25'18.57" W). A) Cliff view. Red dashed box indicates position of photo in part D. B) Line drawings illustrating left-to-right lateral accretion. Red lines highlight plan-view expression of scroll bars. Blue arrows are paleocurrent measurements are trough axes measurements from trough cross-stratification. C) Satellite view of outcrop with paleocurrent superimposed. Note that paleocurrent is parallel to the trend of accretion surfaces. Also note that the rose diagram has been rotated to match the image with north to the right. View for part A is shown. D) Close-up image of outcrop; geologist for scale. The lateral accretion is also visible in this image, top left to bottom right. TCS = trough cross-stratification.

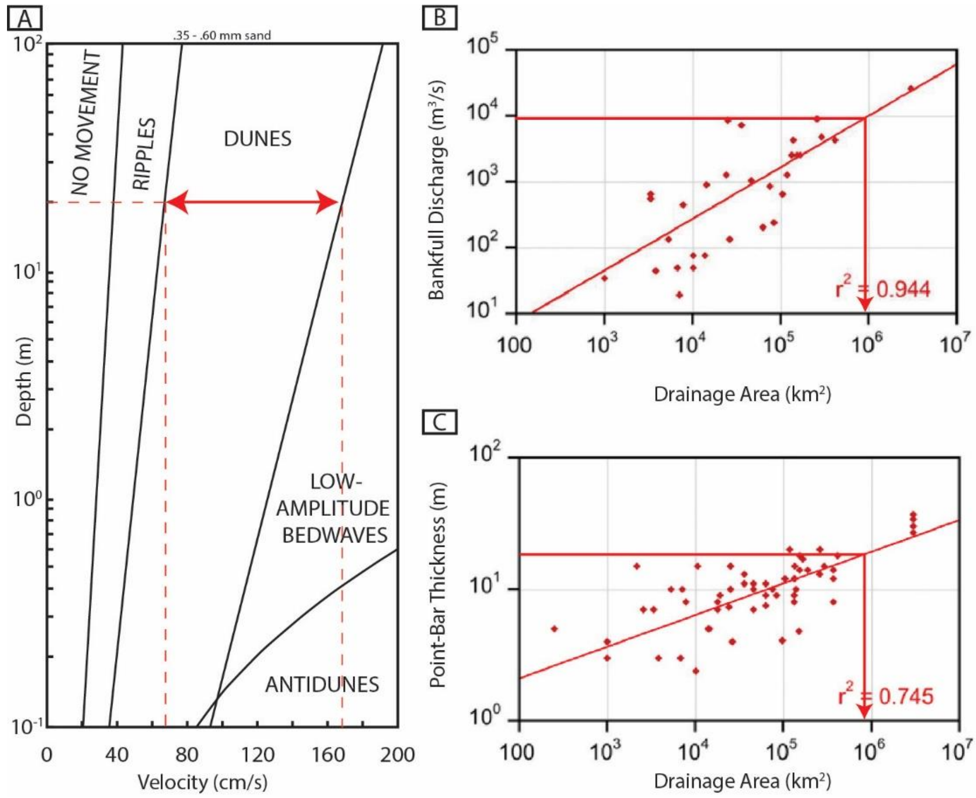

Figure 11: Various plots from the literature used in paleohydraulic calculations. A) Depth-velocity phase diagram for medium sand modified from Rubin and McCulloch (1980) and Bhattacharya and Tye (2004). Velocity range for the thickest bar is shown. B, C) Plots showing the relationship of bankfull discharge or point-bar thickness and drainage area for late Pleistocene to modern single-channel meandering systems modified from Blum et al. (2013). Red lines represent the maximum value obtained from this study. Note that in both instances, drainage area is slightly less than 1 million km^2.

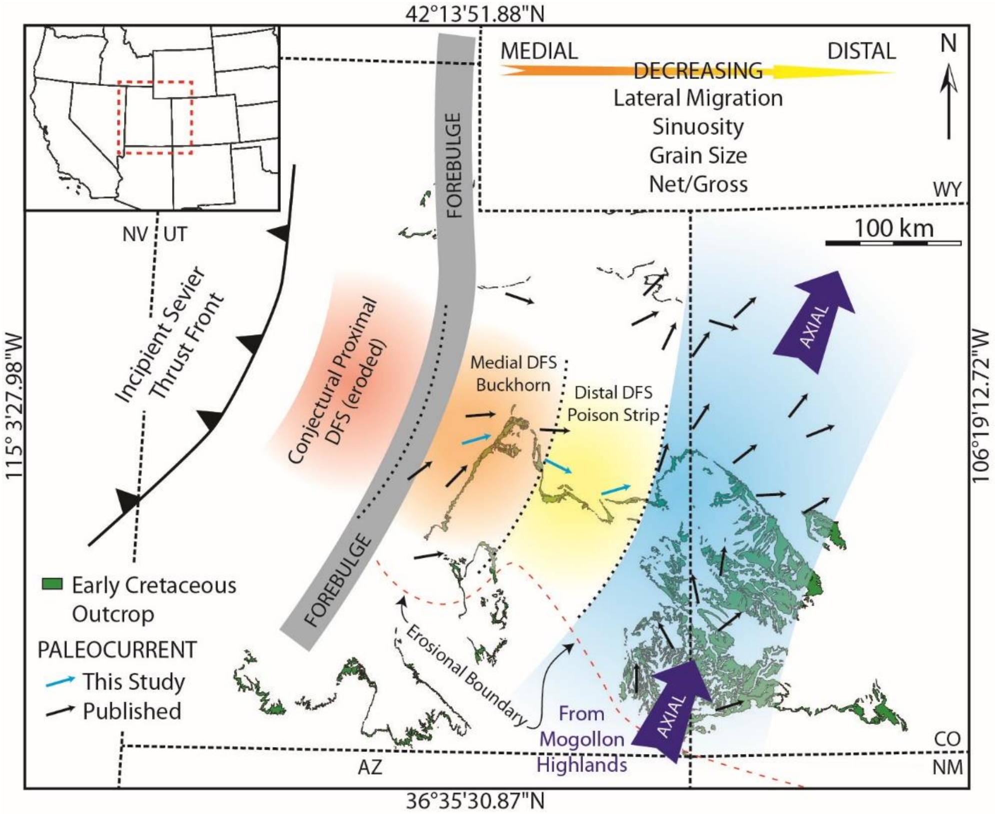

Figure 12: Depositional model for the basal Cedar Mountain Formation. The model depicts a DFS that extends from the thrust front in the west to an axial system in the east. The proximal part of the DFS was removed during erosion of the foredeep deposits. Medial deposits are represented by the Buckhorn Conglomerate, and distal deposits are represented by the Poison Strip Sandstone. Medial-to-distal trends are shown. Paleocurrent data in black were compiled by Dickinson and Gehrels (2008). Position of thrust is from Hunt et al. (2011). Position of forebulge is modified after DeCelles (2004).